J Therm Anal Calorim (2011) 106:285–298
DOI 10.1007/s10973-011-1606-6

Treatment of water-induced curvature of the DSC heat flow rate signal

Applied to fractionated nucleation of polypropylene dispersed in water

Julen Ibarretxe · Gabriël Groeninckx · Vincent B. F. Mathot

NATAS2010 Conference Special Issue

Abstract In samples containing a volatile phase, quite often the evaporation of the volatile substance during heating causes appreciable curvature of the DSC heat flow rate signal as function of temperature, making it difficult to quantify thermal transitions and reorganization phenomena occurring in the same temperature range. This is the case for e.g. polyamide–water, polyamide–alcohol, and polypropylene–water systems, thus complicating the study of polymer crystallization, melting, and metastability by DSC. In this study, maleic anhydride-grafted polypropylene particles of sub-micrometer diameters dispersed in water are discussed. These samples show, upon cooling from the melt, different degrees of extra supercooling in crystallization and several phenomena in the subsequent heating, like reorganization of a crystalline phase into another one, perfecting of crystallites, and melting. All these phenomena are difficult to analyze quantitatively due to the mentioned curvature of the DSC trace. In this article two methods, the "Reference" and "Extrapolation from the melt" methods, are described to correct for the influence of evaporation on the DSC heat flow rate signal and for the baseline signal, enabling the discussion of the transitions by way of the excess heat flow rate as function of temperature.

Keywords Homogeneous nucleation · Polypropylene · Water · Volatile · DSC · Curvature correction

J. Ibarretxe · G. Groeninckx
Division of Molecular and Nanomaterials, Department of Chemistry, Katholieke Universiteit Leuven, Celestijnenlaan 200F, 3001 Heverlee, Belgium

J. Ibarretxe
DSM Research, P.O. Box 18, 6160 MD Geleen, The Netherlands

Present Address:
J. Ibarretxe
Universidad del País Vasco-Euskal Herriko Unibertsitatea, EUITMOP, Beurko s/n, 48902 Barakaldo, Spain

V. B. F. Mathot (✉)
SciTe B.V., Ridder Vosstraat 6, 6162 AX Geleen, The Netherlands
e-mail: Vincent.Mathot@SciTe.nl
URL: www.scite.eu

Introduction

When semicrystalline polymers crystallize, they usually do so by means of heterogeneous nucleation on impurities present in the material and that act as nucleation seeds. These impurities reduce the surface energy of the forming nucleus thus lowering the energy barrier found in the primary nucleation process, and therefore allowing higher nucleation rates at lower supercoolings. Depending on the surface energy between the impurity and the forming nucleus the degree of reduction of the energy barrier varies and therefore each type of of impurity becomes active at a different temperature. A schematic representation is presented in Fig. 1a, where the process of cooling down from the melt is shown. The orange circles represent the heterogeneous nuclei present in the polymer that act as substrates for the formation of the first crystallites.

When crystallization takes place in bulk, the most active impurities trigger the nucleation process, after which growth takes place until the crystallites space-fill the polymer. In this process other, less active impurities might not get the opportunity to trigger nucleation because their activation temperature might not be reached by the time space-filling occurs, as shown in Fig. 1a.

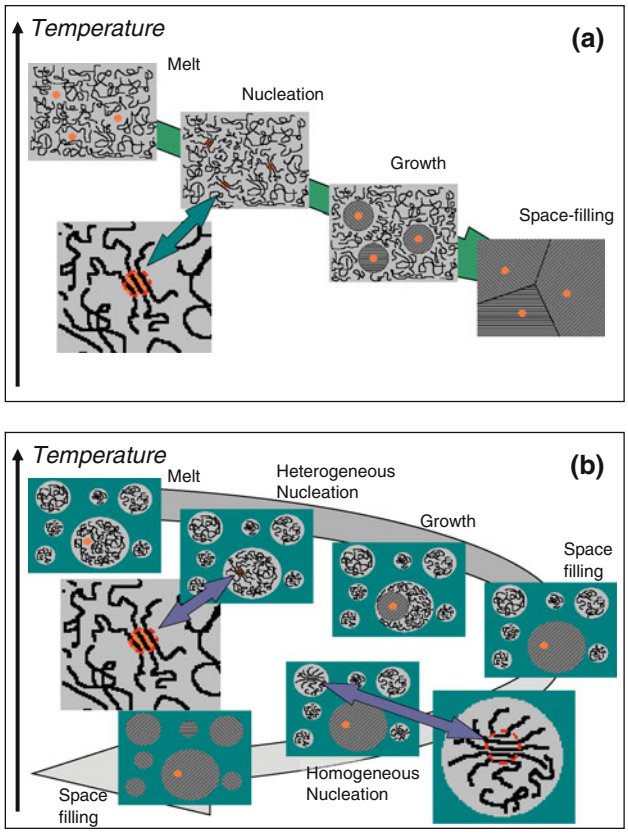

Fig. 1 Schematic representation of the nucleation process in **a** bulk and in **b** a finely dispersed polymer. (Color figure online)

As confronted to heterogeneous nucleation, impurity-free nucleation would take place at a higher degree of supercooling. This process is named homogeneous nucleation. In practice, however, homogeneous nucleation is seldom observed under the usual crystallization conditions because polymers contain important amounts of seeds (catalyst residues, additives, processing aids, and impurities, etc.).

A possibility to observe (and study) homogeneous nucleation is reducing the size of the polymeric sample to such an extremely low value that it does not contain any active impurity. Such size reduction can be obtained by dispersing the polymer into an inert matrix. Depending on the particle size distribution (PSD) of the dispersed polymer, different crystallization behaviors can be obtained in those systems. If the particles are relatively large, they will all contain impurities that become active at the bulk crystallization temperature and therefore the crystallization temperature of the polymer within those particles will not be affected by the dispersion. For somewhat finer dispersions the number of impurities that become active at the bulk crystallization temperature and the number of polymer particles become similar, which yields a system in which many of the particles crystallize at the usual bulk crystallization temperature, but other particles crystallize at lower temperatures. In the latter, the present impurities activate at higher supercoolings. In such a system crystallization proceeds stepwise, and thus it has been named fractionated crystallization [1].

If the particle size is reduced even further some of the particles will be free of any impurity, and they will undergo homogeneous nucleation at very high supercoolings. The crystallization behavior of such a system is shown in Fig. 1b, where a dispersion of a polymer is represented. Heterogeneous nuclei are present in some of the dispersed droplets and trigger crystallization in those droplets at relatively low supercoolings. In other particles no heterogeneous nucleus is present and homogeneous crystallization takes place at higher supercoolings. If the whole polymer is dispersed into extremely fine droplets the vast majority of them will be free of impurities and therefore most of the polymer mass will crystallize homogeneously.

The "droplet method" was initially applied to metals [2, 3], but it was soon adapted to polymer dispersions [e.g., 4–6], polymer blends [see reviews, 1, 7, 8], block copolymers [see review, 9], and more recently also to other types of polymer dispersions [e.g., 10, 11].

Although, initially the droplet technique was developed and mainly used to study the kinetics of nucleation [e.g., 5, 6, 12], over time the different crystallization phenomena observed when this technique was used—namely fractionated crystallization and homogeneous nucleation—gathered more attention [e.g., 13–17] and the most recent studies using this technique have mainly focused on homogeneous nucleation and the effects of confinement on the crystallization process [e.g., 9, 11, 18–20].

Homogeneous nucleation in water-borne dispersions of polymers

In this study, water was used as the dispersion matrix for a maleic anhydride-grafted polypropylene (MA-g-PP). Water was chosen for the matrix mainly due to two reasons. First, part of the interest of using a waterborne polypropylene dispersion lies in the incompatibility between the dispersed polymer and the matrix. Whereas in most of the studies of this type another polymer or a higher-viscosity liquid is usually chosen as matrix, the use of a low-viscosity, highly incompatible liquid can prevent (undesired) surface nucleation phenomena in the polymer droplets [4, 6, 21]. In this type of study, the effect of the matrix is often neglected although it has been shown several times to play an important role in the crystallization behavior of the dispersed polymer [8, 13, 15]. Second, water being an abundant, natural and free resource, it would be of great advantage if it could lead to any application.

If two (or more) immiscible phases are present in the sample the resulting DSC signal is composed of two

(or more) virtually independent contributions, one per phase. This is observed, for example, in the study of polymer crystallization and melting phenomena in multi-phase samples, like immiscible polymer blends [8, 15], immiscible block-copolymers [22, 23], and polymer dispersions in liquids [4, 24, 25]. Irrespective of the independency mentioned, the contribution of one of the phases to the DSC signal can make it difficult to analyze the contribution of the other phase.

When the crystallization of polymers in multi-phase systems is studied, often the polymer phase considered is dispersed in an immiscible matrix, which can be polymeric or not, the latter case being rare. An example of a non-polymeric, immiscible matrix is the system polypropylene-dispersed-in-water—or a "waterborne polypropylene dispersion" —, used here. Several other examples can be found in literature, e.g. [6, 26–29]. Examples of polymer–water systems which can be in a mixed or demixed state depending on temperature and time are polyamide–water systems [30].

It is relatively easy to subtract the contribution of the phase that is not under study from the total DSC signal when that phase is a non-volatile substance and its thermal evolution is known or can be easily measured independently. However, it is not trivial to subtract from the DSC signal the contribution of a volatile substance since its thermal behavior depends on the gas volume inside the DSC pan or sample container, and on the interactions between the different substances present in the sample. It turns out that measuring or calculating the sample's thermal behavior independently can be very difficult. In this article, that matter is treated in detail and two methods for overcoming the problem of quantifying the influence of a volatile phase on the DSC curve are presented.

In addition to the problem described here to analyze the DSC results of samples containing a volatile phase (normally a liquid), a second difficulty can arise when there is some mobility of one of the phases in the sample. Such problem and also a remedy has been discussed in literature [31] for polyamide-solvent systems.

Experimental

Materials

The polymer used in this study is MA-g-PP, Epolene E43, produced by Eastman Kodak. The MA-g-PP contains 7.8 mass% maleic anhydride. The surfactant used is a polyethylene oxide (15) hydrogenated tallowamine, $RN(C_2H_4O)_XH(C_2H_4O)_YH$, where $X + Y = 15$ in average and R is an alkyl group from hydrogenated tallow. The dispersions used here were prepared at temperatures above the melting point of PP and under pressure. The materials were loaded in an autoclave, heated to the desired temperature (175–200 °C), stirred for some 20–40 min, and then cooled down to room temperature. The resulting dispersions range from relatively low viscosity liquids to—in the case of sample S-XI—a very viscous paste. The materials used the method of preparation of these dispersions as well as the PSD of the samples have been discussed in more detail elsewhere [21]. A summary of the composition and particle size of the samples used in the second part of this article is given in Table 1.

Table 1 Composition and particle size data of the dispersions used to illustrate the application of the methods discussed in the Results and discussion section, samples S-I, S-IV, and S-XI

Sample	S-I	S-IV	S-XI
Polymer content/mass%	24.2	29.0	41.5
Surfactant content/mass%	1.3	0	11.8
KOH content/mass%	1.0	2.8	4.0
Water content/mass %	73.4	68.2	42.7
Number average diameter/D_n/μm	4.5	2.1	0.06
Mass average diameter/D_w/μm	52.3	29.4	0.10

Instrumental

For the measurements a PerkinElmer Pyris-1 standard DSC was used. The measurements were performed at 5 °C/min using high purity nitrogen as purge gas in between 0 and 190 °C with 5 min as isothermal stays. High-pressure stainless-steel pans (Perkin Elmer's product number B0182901) were used to ensure that water remains liquid up to the highest measuring temperatures. Empty pan measurements were subtracted from the actual measurements of the dispersions to remove the curvature of the heat flow rate signal as induced by the instrument itself.

Dynamic light scattering (DLS) measurements were performed on a back-scattering set-up (ALV-NIBS High Performance Particle Sizer, ALV Gmbh, Langen, Germany), operating at angle = 173°, at wavelength $\lambda = 632.8$ nm (He/Ne laser, with output power of 3 mW). The conversion of the correlation function into the diffusion coefficient and into the PSD was made automatically by the software.

An Olympus BH-2 optical microscope with a JVC TK-C1381 video camera was used for optical microscopy. A drop of diluted dispersion was put between an object glass and a cover glass for the analysis.

The TEM micrographs were taken on a Philips CM100 transmission electron microscope operating at 80 and 100 KV. A drop of diluted dispersion would be deposited on a Formvar-film grid and left to dry subsequently. For the TEM image presented here, the sample was stained with RuO_4 in solution before depositing it on the Formvar film.

Results and discussion

Water-borne MA-g-PP dispersions

A set of eleven MA-g-PP waterborne dispersions covering a three orders of magnitude range of particle sizes was produced, as reported previously [21]. The DLS determined PSD and the corresponding DSC cooling behavior are shown in Fig. 2a and b, respectively.

The eleven dispersions have been ordered according to their volume average particle size, see Fig. 2a. In Fig. 2b, next to each of the DSC curves the volume and number averages have been added. In those DSC cooling curves important differences between the crystallization behavior of the dispersions can be observed. The different crystallization modes evolve with the PSD of the samples as expected; samples containing only large particles show no extra supercooling because all the droplets contain impurities that activate at the bulk crystallization temperature of the polymer; samples having intermediate size particles display fractionated crystallization because not all the droplets contain the impurities that trigger nucleation at the bulk temperature, but other impurities that become active at lower temperatures. Finally, for samples having very small droplets a very high extra supercooling is observed (77 °C in the case of sample S-XI).

Regarding the DLS data, it must be mentioned that their accuracy is not optimal. The main reasons for the inaccuracy are the large particle sizes present in some of the dispersions, the sometimes broad size distributions and the formation of agglomerates. These errors are especially apparent for the large particle size samples and decreasingly important as the particle sizes in the samples are reduced. For the samples having only small particles the accuracy of the obtained PSDs is correct (see [21] for further details).

Figure 3 presents an optical microscopy (OM) and a TEM image of sample S-IV, which was diluted before the measurements. On the OM micrograph, several features having dimensions above 10 μm are present, which would be expected according to the size data obtained by DLS. However, a careful inspection of these large features found in the OM image reveals that these are not single particles but rather big agglomerates of smaller particles. Since in terms of crystallization behavior—as long as there is no coalescence—the agglomerates do not alter the isolated-particle nature of the polymer droplets, the assessment of the agglomerates as a single big particle is incorrect for the purpose of this study.

Along with the large agglomerates, also smaller, isolated particles are visible in the OM image of sample S-IV. The TEM image of that sample included in Fig. 3b shows with more detail the presence of small particles, some of which may even be below 100 nm.

Heating curves

As it can be observed in Fig. 4, for neat MA-g-PP it is possible to obtain an overall flat DSC curve both in heating and cooling, whereas, regardless of the thermal behavior of the dispersed polymer specific to each sample, the dispersions display a very marked positive curvature in heating and hardly any curvature in cooling. The heating DSC curve of the dispersions can be considered to be the result of adding that of the polymer—which would look similar to the DSC curve of the neat MA-g-PP in Fig. 4a—and the

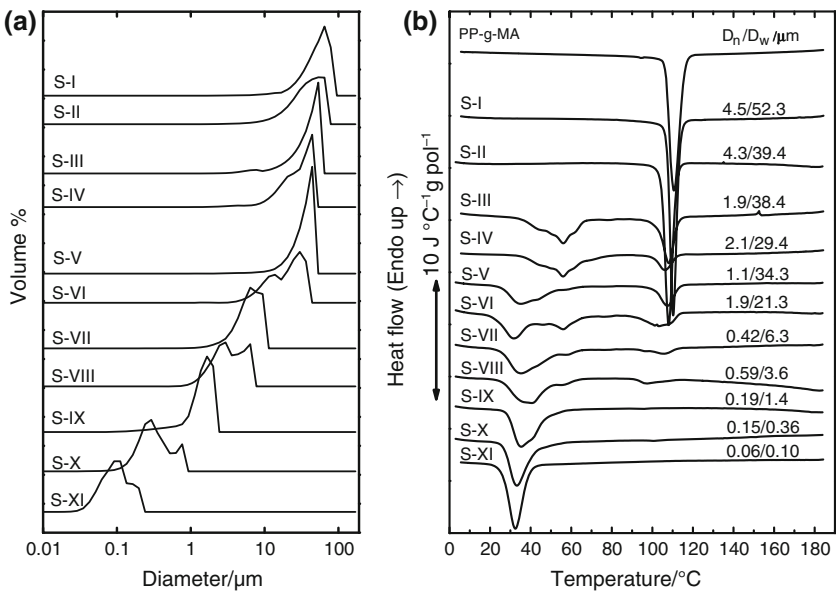

Fig. 2 **a** DLS determined volume percent PSDs of samples S-I to S-XI and **b** their corresponding DSC cooling behavior. In the DSC plot, the curve on *top* corresponds to the trace of the neat MA-g-PP, plotted as reference

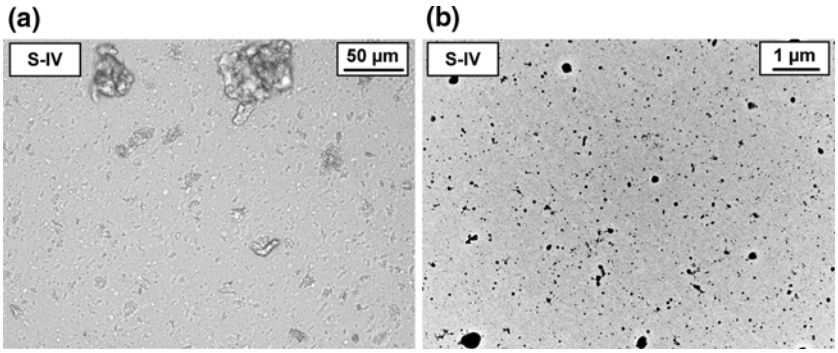

Fig. 3 **a** Optical microscopy and **b** TEM images of diluted sample S-IV

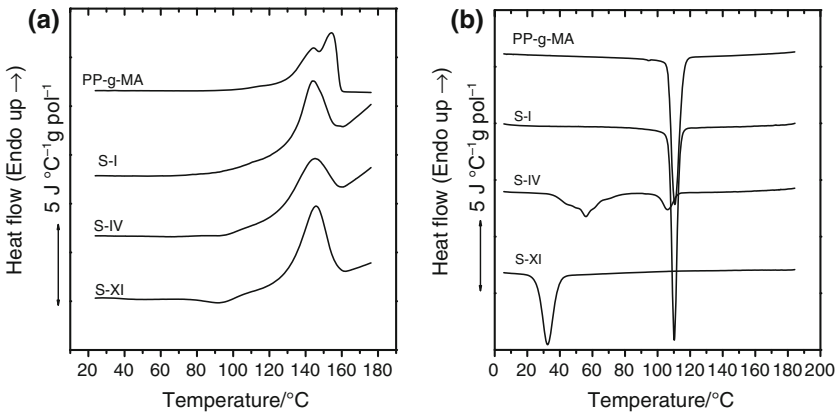

Fig. 4 DSC heating (**a**) and cooling (**b**) curves of the neat MA-g-PP and samples S-I, S-IV, and S-XI

DSC curve of water (see Fig. 5) weighed to their corresponding mass percentages in the dispersion measured. Thus, one could think that to isolate the DSC curve of the dispersed polymer droplets—which is the study subject of this study—it would be possible to perform the same measurement on pure water and then subtract the resulting data from the data obtained for the dispersion.

Indeed, such an approach would be valid for a non-volatile matrix (and on the premise of no influence of the droplets on the thermal behavior of the matrix). However, in case of a volatile matrix subtraction is necessary but not sufficient. In a heating run, a volatile matrix will continuously evaporate due to the increase of its vapor pressure as caused by the temperature rise. Due to the relatively high heat of evaporation of water the total DSC curve is influenced substantially and therefore a small variation of the amount of evaporating water will result in an significantly different DSC curve. Such variations of the amount of evaporated water will take place for different measurements if the volume available for the vapor (the volume that is not taken by the liquid) varies, which depends on the volume occupied by the specific PP–water sample studied.

Moreover, the vapor pressure of a non-pure system not only depends on the vapor pressure of the carrier, but also on the interaction between the solvent and the rest of constituents and on the concentrations of all the substances

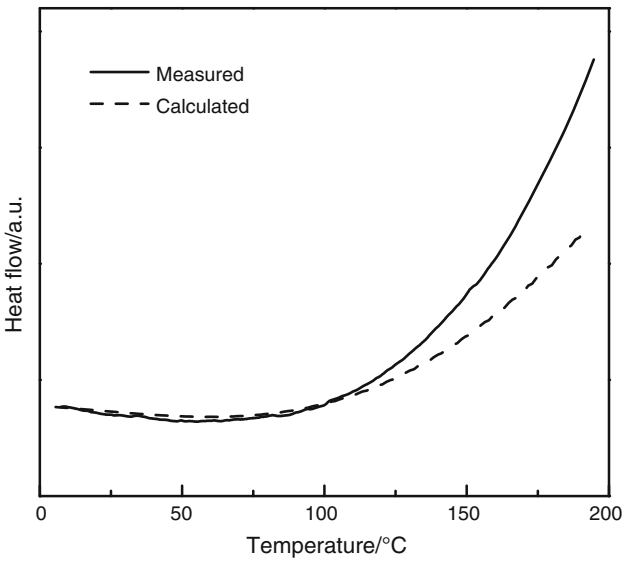

Fig. 5 Calculated and measured heat flow rates in a DSC heating experiment of water in a hermetic, closed pan. The calculated curve has been obtained for the same experimental conditions used in the measurement (sample mass, pan volume, and heating rate) and assuming that the system is continuously in equilibrium

present (the colligative properties and the non-ideality of the solution [32]). Therefore, taking into account all influencing factors, it is virtually impossible to reproduce

the thermal behavior of water in each of the dispersions to obtain a measurement that can be subtracted from the DSC curve of a (MA-g-PP)–water sample to isolate the DSC data of the MA-g-PP.

Similarly, it becomes very difficult to try to calculate the heat flow of the water of the dispersion during a heating or cooling measurement. For pure water, this calculation could still be performed. One must take into account the amount of liquid and vapor at each temperature (for which some assumptions must be made as to the relative humidity or the deviation from the equilibrium conditions) and calculate the total heat flow as the summation of the heat flow due to the evaporation and of the heat flow due to the temperature increase of the sample (through the heat capacity of each of the phases). For the calculation presented in Fig. 5, equilibrium conditions (a relative humidity of 1) were assumed, which is most probably not representative of the process taking place inside the DSC pan. However, a more realistic way to characterize the deviation from the equilibrium conditions in an actual DSC measurement could not be found, and therefore even for pure water it is difficult to realistically simulate its DSC heat flow rate (see the remaining differences between the measured and the calculated curves in Fig. 5).

As mentioned before, the positive curvature observed in the DSC heating scans of samples containing volatile components (e.g., water) impedes the correct analysis of the signal. At the bottom of Fig. 6, sample S-XI is shown as an example of this phenomenon. Sample S-XI is composed of polypropylene particles having dimensions ranging from 10 to 200 nm dispersed in water. It crystallizes at abnormally low temperatures for polypropylene, resulting in the formation of a low stability mesophase instead of the more stable and common α phase. In the DSC heating curve of this sample there are clear features present (see the exotherm from approximatively 35 to 110 °C and the melting peak around 150 °C) that cannot be analyzed quantitatively with respect to the enthalpies involved due to the overall curvature of the DSC trace.

For correction of the curvature of the signal during the heating scan, a reference signal having exactly the same positive curvature must be used. Such a reference has been indicated manually by a dashed line in the DSC curve at the bottom of Fig. 6. This "correction curve" should account for the heat flows as related to the heat capacities of liquid and gaseous water; for the enthalpy of evaporation of water; and for the heat capacity of the polymer without phase transitions, all these quantities being temperature dependent. After subtraction of such a correction curve from the actual DSC curve, only the heat flow due to the excess heat capacity as caused by phase transitions in the polymer would remain. Such a correction curve has been named "baseline" in literature [33].

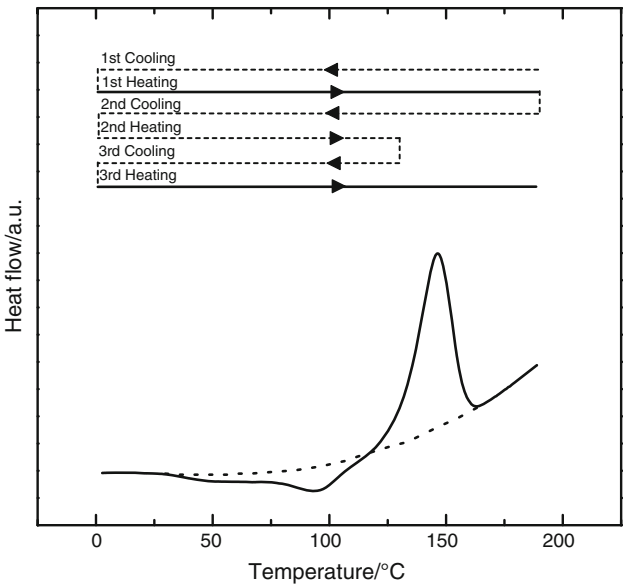

Fig. 6 DSC first heating curve of sample S-XI (*bottom part*) and the temperature-time ramps applied for the correction of the curvature (*top part*). The isothermal stays took 5 min at 0 and 190 °C and also at the annealing temperature, 137 °C

Because a rigorous solution for obtaining the correction curve has not been found, in a "first approximation approach" the sample itself is used to create the correction curve. To this end, the sample is treated in such a way that a heating, reference measurement of the sample can be performed in which all the first order thermal transitions of the polymer take place in a as narrow temperature range as possible. Then, part of the resulting reference curve is used as correction curve after removal of the part where the thermal transitions of the polymer take place, as will be explained in the following.

By heating the sample to 190 °C, an isothermal stay of 5 min and cooling to 0 °C, it is given a thermal history. Next, the first heating curve is measured as presented in Fig. 6. Then, the sample is cooled from the melt to the lowest temperature (0 °C in this case), and subsequently heated and annealed for a long enough time at a temperature above the temperature range where the transformation of the mesomorphic to α phase takes place (from approximately 80 °C on, followed by reorganization of the latter phase till approximately 120 °C—see [34] for details—as visible as exothermic events in the DSC curve), but still below the temperature range of final melting. The annealing temperature chosen here is 137 °C. Then it is again cooled down to the lowest measuring temperature. In this way, when the sample is cooled down from the annealing temperature it will not show crystallization since the crystallites that formed during the first cooling run are still present. Subsequently, the sample is heated up until the final melting temperature is reached. During this (third)

heating run there will be melting, but no exotherm process and concomitant reorganization are expected anymore until the annealing temperature is approached. Thus, the phase transitions will take place in a relatively narrow temperature range if compared to the original, actual measurement. The data recorded in this final heating run will be used to obtain the approximate correction curve. The top part of Fig. 6 presents the temperature–time ramps applied to the sample in this example, showing which runs are used as actual measurement (first heating run) and as base for creating a correction curve (third heating run), both of them solid lines.

It is important to point out that for the use of this approach the samples must be thermally stable. In this way there will be no variation of the thermal behavior of the samples while the heating and cooling measurements take place, and an adequate correction curve can be constructed. In this regard, the MA-g-PP dispersions used here have proven to be thermally very stable systems and the temperature profile applied to them does not alter their PSD [21]. Therefore, their thermal response during the DSC measurements is completely repeatable, which allows to apply this kind of method.

The correction curve is obtained by performing a third order polynomial fit of the data of the third heating, reference curve, excluding the range of data where melting occurs. In the case of sample S-XI, the range chosen for the fitting was 0–100 °C and 162–195 °C. In that range the signal only shows the curvature due to the evaporation of water since the previous annealing step prevents subsequent (cold) crystallization and reorganization at lower temperatures. The so-obtained correction curve turns out to be situated lower than the actual curve at the lowest temperatures (see Fig. 7) although this method is applied to obtain a correction curve that equals the measured data at those temperatures. The explanation is that the correction curve—attained by a fit of the third heating, reference curve—was obtained from a sample having solely the α phase as crystalline phase with—due to the annealing step—a higher degree of crystallinity than in case of the actual measured DSC curve which, at low temperatures, reflects the mesophase and a lower crystallinity. Thus, the specific heat capacity of the reference curve will be lowered compared to the actual curve because of the higher crystallinity [33], as is the heat flow in Fig. 7. Since in the measurement performed to obtain this reference curve the crystallinity is higher than in the actual curve from 0 to a few degrees above 137 °C (because the effects of the annealing step disappear a few degrees above the annealing temperature which is 137 °C in this case) the error introduced in the corrected data will also cover that temperature range.

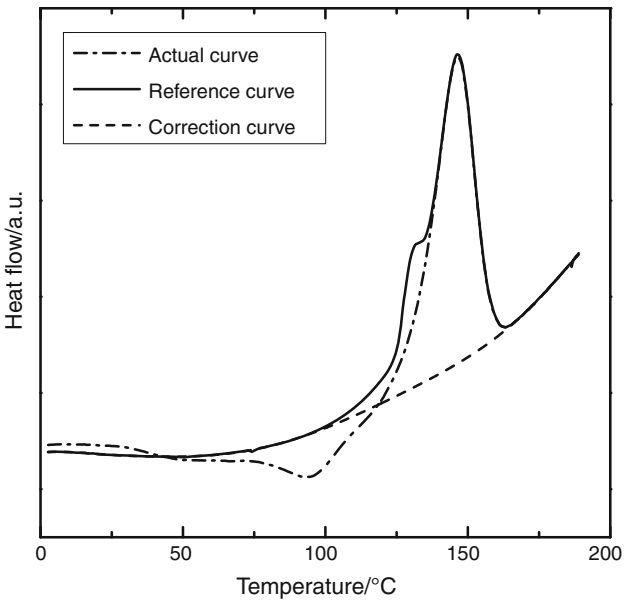

Fig. 7 Actual curve (*dashed-dotted line*), reference curve (*solid line*), and correction curve (*dashed line*) for sample S-XI. The correction curve was obtained as a polynomial least-squares fit to the 0–100 °C and 162–195 °C temperature ranges of the reference curve

The high temperature range of the reference and the correction curves will be accurate since above 160 °C the physical state of the polymer in both actual measurement and reference measurement is exactly the same.

The fitting of the reference curve is shown in Fig. 7 (dashed line), as well as the result of subtracting it from the actual measurement (solid line). If the obtained corrected curve were entirely accurate, the regions where there is no phase transition (no excess-heat flow) would appear at the zero level. By applying the correction to sample S-XI, the corrected curve is situated at the zero level in the melt. However, the preliminary result obtained is indeed situated above the zero level for temperatures between 0 and approximately 30 °C, where the sample is known not to undergo any phase transition (as observed in time resolved X-ray measurements that will be published in a separated article). This deviation is caused by the difference between the actual measurement and the reference curve in this temperature range, as explained above, and it also affects all the temperature range up to around 137 °C.

As remarked before, because obtaining a rigorous solution for the correction curve is not feasible and was not sought for any longer, a further correction procedure to bring the outcome at low temperatures also to the zero level (like for the melt) was performed by simple subtraction. The preliminary result shows a constant deviation from zero between 0 and 30 °C (the difference after subtraction is practically constant). From there to 137 °C

(temperature above which the correction is all right) the preliminary result lies gradually closer to the actual measured curve since further crystallization and reorganization into the α phase occur in the sample (these results will also be published separately). In order to finalize the process of obtaining a reasonable approximation of the baseline an assumption must be made as for the rate of diminution of the error induced in the corrected curve from 30 to 137 °C, since the actual shape of the baseline is not known for that temperature range. In this case, a straight line has been chosen meaning that the error of the preliminary result diminishes linearly from 30 to 137 °C. Although this choice is maybe not realistic, the error induced is anyhow so small that the effect of choosing another type of function will almost not affect the final result.

Therefore, from 0 to 30 °C a constant value equal to the deviation from zero has been subtracted from the preliminary result, and from 30 to 137 °C a starting value equal to the deviation at 30 °C decreasing in a linear manner down to zero at 137 °C has been subtracted (dashed line in Fig. 8). The final result (dashed-dotted line in Fig. 8) shows the two regions where no phase transitions of the polymer occur at the expected zero level. It has to be emphasized that only subtraction of the correct baseline heat flow from the measured sample heat flow would result in the excess heat flow [33]. However, for the moment, as a first-order approximation it is considered that the present final result is a reasonable estimate of this excess heat flow.

Figure 9 presents the results of the same treatment applied to samples S-I, S-IV, and S-XI, together with the original

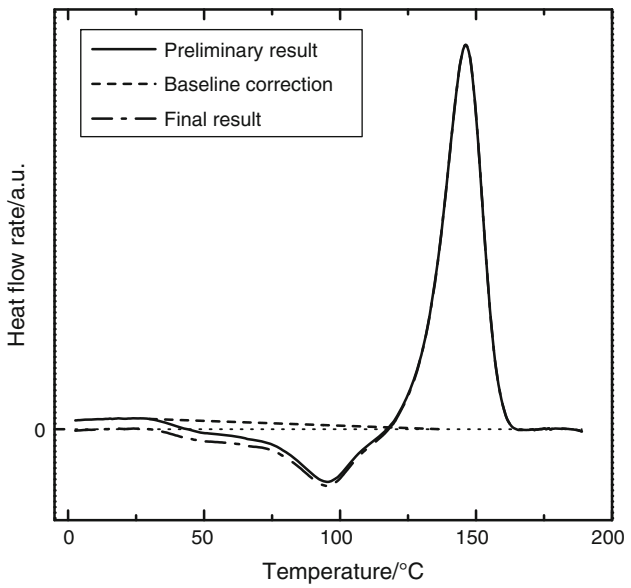

Fig. 8 Results of the subtraction of the fitted reference to the measurement (*solid line*), correction for the difference in crystallinity (*dashed line*), final result after correction (*dashed-dotted line*), and zero level indicator (*dotted line*)

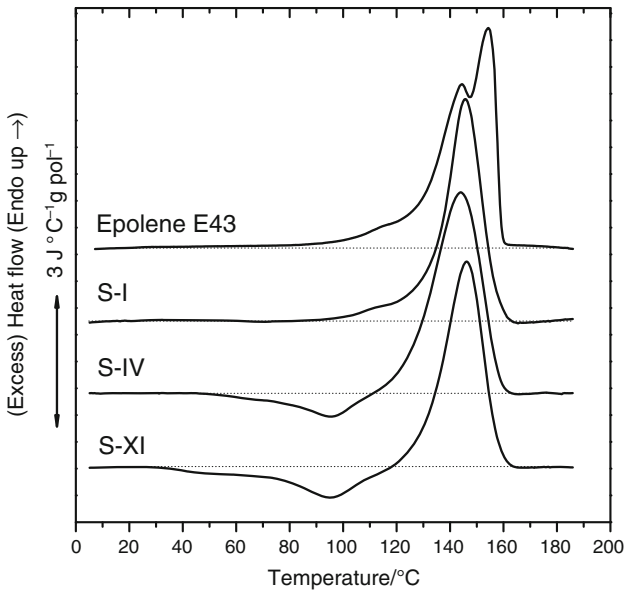

Fig. 9 DSC excess heat flow heating curves of the neat MA-g-PP and the three dispersions after correction of their curvatures. The zero level is represented by the *dotted lines*

DSC curve for the neat MA-g-PP. It has to be pointed out that for sample S-I it was not necessary to bring the data at low temperatures to the zero level because the reference curve and the actual curve were approximately at the same level. In fact, in sample S-I the crystallinity is naturally higher (see the Application section) and there is no mesophase, but just α phase, and therefore the effect of the annealing step to the crystalline microstructure is not very significant. Thus, in this case the correction curve obtained by fitting the third heating DSC curve yields a good approximation of the baseline for that sample, which could hold a very small error due to an eventual little crystallinity difference between the reference and the actual measurement.

Cooling curves

Although plain water measured in cooling in a DSC pan displays a behavior similar to that of the heating curves, i.e., a very curved DSC trace due to the continuous condensation during the cooling process, paradoxically it does not display such a marked behavior for the dispersions discussed here as can be observed in Fig. 4b. In fact, the dispersions do not show an important curvature, and seemingly condensation does not take place extensively. A similar asymmetry in the heating and cooling DSC curves can be observed in the study performed by Landfester et al. on emulsions of several alkanes in water [27], whereas in another study performed by that same group on emulsions of poly(ethylene oxide) in water also the cooling DSC data show marked curvatures [28].

This anomalous thermal behavior of the matrix in the dispersions must be related to the deviation from equilibrium during the cooling DSC measurement, where the condensation must be delayed considerably. Undoubtedly, the interaction between the constituents of the dispersions plays a very important role in this process, as pointed out before.

However, if the condensation of the volatile matrix during the cooling measurement showed the expected highly visible curvature of the DSC trace, one could apply the method used in heating to obtain a "correction curve" also in the case of the cooling runs. For example, if this method was applied to sample S-XI in cooling the employed program could consist of a first complete cooling ramp (which would be the actual measurement), a heating ramp to a temperature below the beginning of the final melting (100 °C for example), and then a cooling ramp that would be used as reference and in which no crystallization would take place. Proceeding in such a way one would obtain a reference curve whose heat flow, once again, would be slightly lower than the heat flow of the actual curve in some temperature range due to the crystallinity difference. Again, that deviation could be treated to obtain the correction curve that by subtraction to the actual curve would provide a good approximation of the excess heat flow of the process.

In addition to the "Reference method", a second curvature correction procedure can be implemented for the case of the cooling curve of sample S-XI, as will be explained below. For the univocal analysis of the phase transitions reflected in a DSC curve one can apply the "Extrapolation from the melt method" reported in literature [33] using a two phase system. In this approach, the DSC curve is extrapolated from the melt to lower temperatures (to the temperature range where the phase transition takes place, and below that). This extrapolation from the melt should be done using a straight line if suitable, but in case the DSC trace presents any curvature in the melt region an extrapolation can be tried using a second-order polynomial function. Then, by integration of the area between the measured curve and the extrapolated curve and comparison of that integrated area ($[A_1 - A_2]_T$, as shown in Fig. 10) to the reference enthalpy of transition of the polymer ($\Delta h_{\mathrm{ref}}(T)$) at the temperature of interest, one can obtain the crystal fraction of the polymer at any temperature ($w^{\mathrm{c}}(T)$), according to Eq. 1.

$$w^{\mathrm{c}}(T) = \frac{[A_1 - A_2]_T}{\Delta h_{\mathrm{ref}}(T)} \tag{1}$$

Then, the excess specific heat capacity ($c_{p_{\mathrm{e}}}(T)$) of the transition can be obtained according to the following expression:

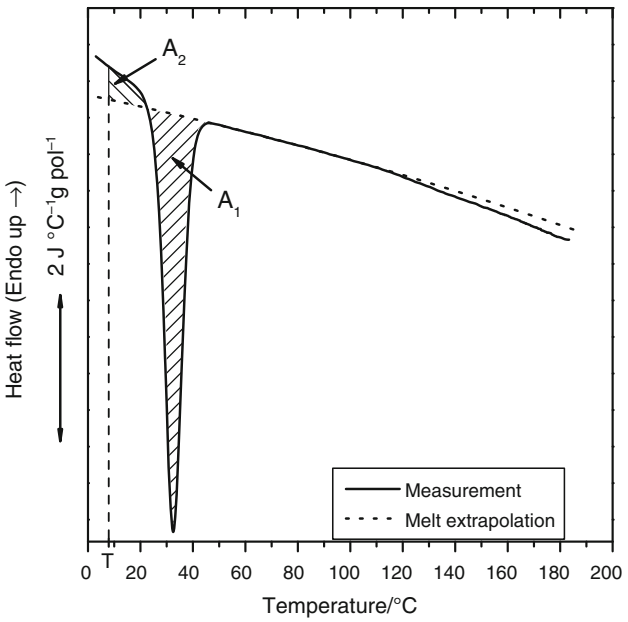

Fig. 10 DSC heat flow of the cooling curve of sample S-XI (*solid line*) and extrapolation from the melt (*dotted line*). The integration areas (A_1 and A_2) are also shown for an integration temperature T below the transition temperature range

$$c_{p_{\mathrm{e}}}(T) = -\Delta h_{\mathrm{ref}}(T) \cdot \mathrm{d}w^{\mathrm{c}}(T)/\mathrm{d}T \tag{2}$$

Once $c_{p_{\mathrm{e}}}(T)$ is known the heat flow of the baseline, $(\mathrm{d}q/\mathrm{d}T)_{\mathrm{b}}$, can be calculated since

$$(\mathrm{d}q/\mathrm{d}T)_{\mathrm{measured}} = (\mathrm{d}q/\mathrm{d}T)_{\mathrm{b}} + c_{p_{\mathrm{e}}}(T) \tag{3}$$

where $(\mathrm{d}q/\mathrm{d}T)_{\mathrm{measured}}$ is the measured heat flow. At this point the phase transition is—thermally speaking—completely characterized. This is the method that will be followed to analyze the cooling DSC curve of sample S-XI. The reader is directed to the original text for a fuller explanation of this procedure [33].

As can be seen in Fig. 10, the cooling DSC curve of sample S-XI presents some problems when it comes to its analysis. First, the curve has a sudden change of slope around 110 °C. Second, the part of the curve immediately above the phase transition (50–100 °C), which will be used for extrapolation to lower temperatures, is not linear, in contrast to expectation for a polymer. Finally, after the curve in the melt region has been extrapolated, it could appear—to the eyes of the experienced DSC analyst—that the rate of departure of the measured curve from the extrapolation line from the melt is uncommonly high in the temperature range below the phase transition temperatures. This deviation, as will later be confirmed, is problematic to have an accurate analysis, and it will require a special treatment.

Probably, all three irregularities of the DSC cooling curve are related to the other constituents of the sample that accompany the polymer, i.e., water and surfactant.

Although, as mentioned above, the overall curvature of the DSC curve is much less marked in the cooling curves than in the heating ones, it appears that the influence of the other components of the sample on the DSC curve cannot be disregarded altogether. Therefore, in this second curvature correction method, a few adjustments to the data were necessary to improve the feasibility of the analysis and finally reach a good estimation of the excess heat flow (or excess specific heat capacity) of the polymer during the cooling process. Before doing so, it has to be stressed that the DSC cooling curve as shown in Fig. 10 is fully reproducible: the irregularities discussed are not caused by instrument failures.

The first action to adequate the measured data for the analysis was to completely neglect the data above 100 °C. Since the only phase transition that takes place during the cooling measurement starts at around 44 °C, ignoring the data above 100 °C does not interfere in the analysis of that transition. Also, this reduction of the data points in the melt region does not pose any problem when it comes to the melt extrapolation for sample S-XI because there is still a wide temperature range (50–100 °C) from which the extrapolation can be accurately done. Therefore, this method is especially suited for cooling curves because the supercooling usually provides a long-enough temperature range for extrapolation.

The second applied measure was to use a second-order polynomial extrapolation of the melt, instead of the expected straight-line, to consider the curvature provided to the DSC data by the other constituents of the sample. This procedure is mandatory to obtain an extrapolation from the melt that corresponds (as much as possible) to the heat flow of the amorphous phase of the polymer plus the curvature conferred by the heat flow of the other constituents. The resulting extrapolation line is shown in Fig. 10 (dashed line).

Then, $[A_1 - A_2]_T$ was calculated by integration from the melt to a certain temperature T. For T temperatures above the temperature where the measured curve and the extrapolation from the melt cross (named T^* in literature, and which corresponds to 22.5 °C in this case), A_1 is taken as the partial area while A_2 is zero. Combining the integration results with the reference enthalpy data for the amorphous to mesophase transition—$\Delta h_{\mathrm{ref}}(T)$, to be published shortly—$w^{\mathrm{c}}(T)$ was then calculated. Finally, determining $\mathrm{d}w^{\mathrm{c}}(T)/\mathrm{d}T$ allowed to compute the excess specific heat capacity and the baseline specific heat flow of the sample by applying Eqs. 2 and 3 respectively, which are shown in Fig. 11 as "preliminary" results.

It is evident from the plotted curves that the preliminary baseline and $c_{p_{\mathrm{e}}}(T)$ are incorrect. A correct $c_{p_{\mathrm{e}}}(T)$ would be zero at the lowest temperatures where no phase transition takes place, but the preliminary $c_{p_{\mathrm{e}}}(T)$ visibly differs from zero. In addition, a correct baseline would match the measured heat flow data in that same temperature range, which is not the case here. This error is most certainly due to the effects of the water and surfactant on the heat flow curve, causing the—previously mentioned—uncommonly high rate of departure of the measured data from the extrapolation line from the melt. Moreover, the possible formation of the rigid amorphous fraction (RAF) of iPP in that temperature range could also affect the heat flow curve. Without further investigation the extent of each of these two phenomena cannot be quantified.

In order to rectify this deviation from the correct curve shapes of the $c_{p_{\mathrm{e}}}(T)$ and $(\mathrm{d}q/\mathrm{d}T)_{\mathrm{b}}$, the error observed in the excess specific heat capacity curve was used to obtain a new extrapolation from the melt curve. This new extrapolation for the melt was such that it yielded correct-shape $c_{p_{\mathrm{e}}}(T)$ and $(\mathrm{d}q/\mathrm{d}T)_{\mathrm{b}}$ curves. The so-corrected final results are presented in Fig. 11 as "corrected".

The first step of the procedure to obtain the new extrapolation from the melt curve was to perform a (polynomial) fitting of the parts of the preliminary $c_{p_{\mathrm{e}}}(T)$ curve where there is no phase transition (3–19 °C and

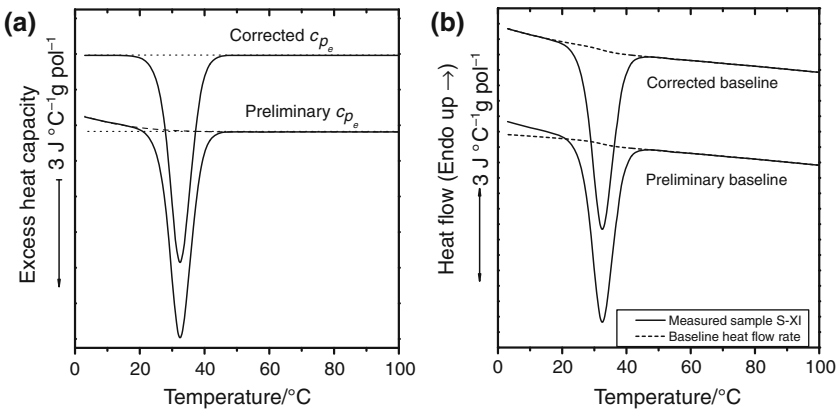

Fig. 11 **a** Preliminary and corrected excess heat capacity curves, where the zero level is represented by the *dotted lines*. The dashed trace shown along the preliminary excess heat capacity curve represents the error of that curve which is used to derive a corrected extrapolation from the melt. **b** Preliminary and corrected baseline heat flow curves in cooling by DSC of sample S-XI (*dashed lines*)

50–100 °C in this case), as shown (by the dotted line) for the "preliminary $c_{p_e}(T)$" curve in Fig. 11a. This fit represents the absolute error in the $c_{p_e}(T)$ curve and if it were directly subtracted to that curve an accurate estimation of the actual $c_{p_e}(T)$ would be obtained, from which $(dq/dT)_b$ could be calculated using Eq. 3.

However, the results presented here were obtained following a lengthier path for the reasons that are explained below. Once that error was fitted, the obtained polynomial function was treated according to the "Extrapolation from the melt method", but in reverse order. So in this case, starting with an (error) excess specific heat capacity, the corresponding $dw^c(T)/dT$ was obtained by means of Eq. 2. Then $w^c(T)$ was calculated by integration of $dw^c(T)/dT$, and, using Eq. 1, $[A_1 - A_2]_T$ could be determined. Finally, the heat flow corresponding to the error in the excess heat capacities was derived by differentiating $[A_1 - A_2]_T$.

Subtracting the heat flow corresponding to the error from the previously used extrapolation from the melt resulted in a new curve that was used as new extrapolation from the melt. Using this new curve as integration reference for the re-calculation of A_1 and A_2, and taking all the subsequent steps in the method used before, finally the "corrected" $c_{p_e}(T)$ and $(dq/dT)_b$ shown in Fig. 11 were calculated.

The reason why this lengthier path for the recalculation of $c_{p_e}(T)$ was chosen is that, although here $\Delta h_{ref}(T)$ has been considered to be known for the forming crystalline phase during the cooling experiment, in reality those data have never been reported in literature. However, the data treatment procedure presented here was used to estimate $\Delta h_{ref}(T)$ through an iterative calculation process that required the reverse calculation path to be used.

The procedure shown here for the correction of the anomalous features displayed by sample S-XI in the DSC cooling trace (the sudden change of slope in the melt region, the overall curvature, and the too marked slope difference between the regions above and below the transition temperatures) is highly reproducible. Besides, the shape of the obtained $c_{p_e}(T)$ curve is completely appropriate, and this—per se—is an indication of the adequacy of the estimation obtained by the method. Again it has to be stressed that the experiments are highly reproducible too, excluding instrumental failures.

Figure 12 presents the excess heat capacity and corrected, measured/baseline curves for samples S-I, S-IV, and S-XI (estimated using the "Extrapolation from the melt method") and the neat MA-g-PP.

Application

As mentioned before, the results of using the first curvature correction method presented here ("Reference method") on some of the water-borne MA-g-PP dispersions are shown in Fig. 9 and the results of using the "Extrapolation from the melt method" in cooling are shown in Fig. 12. From the excess heat capacity curves obtained, one can easily calculate the excess enthalpies, which are presented in Table 2.

If the integration results, as shown in Table 2, are analyzed one can observe that there is a non-significant difference in the results for the endothermic and exothermic processes in the case of the neat MA-g-PP and sample S-I, but that the difference becomes increasingly significant for samples S-IV and S-XI. Notice that for the latter samples, the enthalpies of the endothermic transitions, i.e., melting, are larger than the enthalpies of the exothermic transitions. This is the expected behavior due to the temperature dependence of the heats of transition [33]. Those heats become smaller for decreasing temperatures (also in the case of the amorphous to the monoclinic phase transition [35]), and in general the enthalpies involved in the transitions taking place at higher temperatures (melting in this case) are higher than the enthalpies of the transitions taking place at lower temperatures (crystallization and reorganization/cold crystallization). Since for the neat MA-g-PP the gap between the crystallization and the melting temperatures is relatively small, also the influence of the

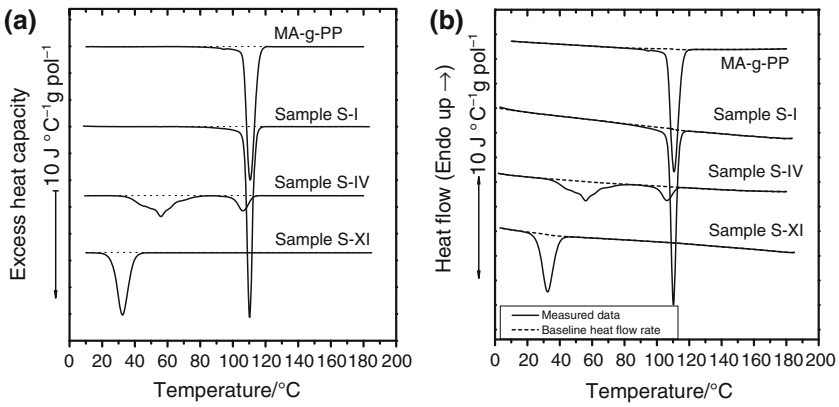

Fig. 12 **a** Excess heat capacity curves—and their corresponding zero level represented by the *dotted lines*—and **b** corrected, measured/baseline heat flow curves in cooling by DSC of samples S-I, S-IV, and S-XI, as well as for the neat MA-g-PP as based on the "Extrapolation from the melt method"

Table 2 Enthalpies of transition obtained from the integration of the DSC curves for the neat MA-g-PP and the three dispersions after correction of the curvature in the DSC traces

Specific enthalpies of transition/J g^{-1}	MA-g-PP		S-I		S-IV		S-XI	
	Endo	Exo	Endo	Exo	Endo	Exo	Endo	Exo
Heating	78		76		65	11[a]	83	26[a]
Cooling		77		77		36[b]		49
						12[b]		
Total	78	77	76	77	65	59	81	75

The enthalpies of the different phenomena (crystallization, reorganization/cold crystallization, and melting) are separated according to the type of DSC curve they are measured in (heating—Fig. 9—or cooling—Fig. 11a) and the thermal nature of the process (endothermic or exothermic). The results are given in J/g of polymer

[a] Due to reorganization/cold crystallization during heating

[b] Several crystallization peaks during cooling

temperature dependence of the enthalpies is small. When the temperature difference between crystallization and melting increases also the enthalpy difference between the endothermic and the exothermic processes increases, as can be seen in the case of samples S-IV and S-XI. Therefore, correcting the results for the mentioned temperature dependence of the enthalpies becomes necessary for the validation of the curvature correction method used.

While the thermal properties—and thus the evolution of the enthalpy of transition with temperature—of crystalline and amorphous PP can be found in literature [35], this source presents a single set of data for the crystalline phase. Given that each crystal modification has its own thermal properties, to make it thoroughly complete there should be a set of data for each of the four known crystalline modifications of PP (monoclinic or α, hexagonal or β, orthorhombic or γ, and mesomorphic). The data for the crystalline phase given in the ATHAS database correspond to the monoclinic crystal structure, as confirmed to us by its authors.

Out of the four sets of DSC data presented in this article, the neat MA-g-PP, sample S-I, and (probably) sample S-IV crystallize solely in the monoclinic form, as observed by WAXD measurements (to be published). There might also be a little formation of the mesophase in sample S-IV, but very small in any case. On the other hand, sample S-XI crystallizes entirely in the mesomorphic form upon cooling, then upon heating the mesophase formed in the cooling run extends further and subsequently it reorganizes into the monoclinic form, which finally melts. In order to correct for the temperature dependence of the enthalpy of transition of that sample, all the mentioned crystallization and reorganization phenomena must be thoroughly analyzed and quantified. In the case of the neat MA-g-PP and samples S-I and S-IV the enthalpies of transition were converted to variations in crystallinity using Eq. 4 to carry out that correction. Due to the discrete nature of the used data, this equation is expressed as a summation:

$$\Delta w^{c}(T_{\text{final}}) = \sum_{T_{\text{initial}}}^{T_{\text{final}}} \frac{\Delta h_{\text{measured}}(T_i)}{\Delta h_{\text{reference}}(T_i)} \tag{4}$$

where $\Delta w^{c}(T_{\text{final}})$ is the absolute crystallinity variation, $\Delta h_{\text{measured}}(T_i)$ is the measured enthalpy of transition corresponding to temperature T_i, $\Delta h_{\text{reference}}(T_i)$ is the reference enthalpy of transition for PP at temperature T_i calculated as the enthalpy of the amorphous phase minus the enthalpy of the crystalline phase (as provided in [35]), T_{initial} is the starting temperature of the transition being considered and T_{final} is the end temperature of that transition.

Table 3 Crystallinity variations (%) calculated from the corrected DSC data (Figs. 9, 12a) and taking into account the temperature dependence of the enthalpy of transition in crystallization and melting

Crystallinity/%	Endothermic	Exothermic
MA-g-PP	39	40
S-I	38	40
S-IV	33	33

The "endothermic" column represents the crystallinity variation observed due to the endothermic processes (melting) and the "exothermic" column represents the total crystallinity variation due to the exothermic processes (crystallization and reorganization/cold crystallization) during the heating (Fig. 9) and cooling (Fig. 12a) runs

Table 3 shows the results of the use of Eq. 4, which are presented in terms of the crystallinity development during the exothermic transitions—i.e., crystallization and cold crystallization plus reorganization—and crystallinity reduction during the endothermic transitions—i.e., melting—taking place in the polymer in the course of the cooling and heating experiments.

As can be observed in Table 3, there is a fairly good agreement between the crystallinity variations calculated for the endothermic and exothermic processes for the neat

MA-g-PP and the dispersions. The observed error is similar for a system in which the correction method for the curvature was not used (i.e., neat MA-g-PP) and for the systems in which it was used, i.e., samples S-I, S-IV, and S-XI. Thus, the applied correction methods give consistent results and seem to be adequate to obtain the sought outcome.

The results for sample S-XI will be published separately because to correctly analyze the transitions taking place in that sample the enthalpy of the mesophase must be known over a wide temperature range. In future article, we will present an estimation of that enthalpy between 0 and 200 °C—which has not been published before—and the use of the correction methods described in this article on sample S-XI will be shown as well.

Conclusions

When DSC cooling or heating experiments are performed in polymer-in-a-volatile-matrix systems, the volatile substances condense (in cooling) or evaporate (in heating) due to the vapor pressure variation induced by the change in temperature, resulting in curved DSC signals. Such curvature covers the entire experimental temperature range, superimposing on the rest of the thermal phenomena and it renders the quantitative analysis of the phenomena related to the non-volatile phase very difficult. According to our observations, the curvature induced by the condensation of water during cooling is much smaller than in case of evaporation during heating.

Even in case the constituents form immiscible phases the resulting signal is not only made up by the contributions of these phases. In addition, it is also influenced by the interactions between the different substances across the phase boundaries present, by the volume at the disposal of the volatile phase inside the DSC pan, etc. Thus, measuring or calculating a background DSC signal that could be subtracted from the measurement results to isolate the signal corresponding to the non-volatile (polymeric) phase is very problematical.

Two possible—(semi)empirical—solutions are presented for the polypropylene–water system. The first solution, by way of the "Reference method", is based on the subtraction, from a DSC actual curve, of the contribution of the evaporation (or condensation) of the volatile substance and the heat required (or released) by all the substances in the sample during heating (or cooling). The approach adopted consists of experimentally obtaining an empirical "correction curve" by annealing at relatively high temperature. This correction curve is an approximation of the "baseline" of the DSC measurement [33]. The correction curve can be subtracted from the actual curve to obtain the excess heat flow curves. Depending on the thermal transitions present in the sample this approximation can yield a highly precise corrected curve.

This "Reference method" can be applied to any system having a wide temperature range in which a "correction curve" like the one described can be empirically calculated. This is valid for any DSC measurement of a multiphase system for which intrinsically, or by means of a thermal treatment, the excess heat flow is restricted to a narrow temperature range. It can then be applied to both heating and cooling curves. In this article, DSC heating curves were chosen to show the use of this procedure.

The second solution to the curvature problem is based on the "Extrapolation from the melt method" to univocally analyze the DSC traces of polymeric samples undergoing a phase transition using a two-phase model [33]. Combining this analysis method with a few adjustments to the DSC cooling trace allowed to obtain an estimate of the excess heat capacity of the polymer and the baseline of the measurement in the range of temperatures covered by the DSC data. This procedure is essentially more suitable for DSC traces displaying curvatures (due to the presence of other substances in the sample) that are not very apparent, rather than for highly distorted DSC traces where the extrapolation from the melt can be very difficult. The use of this second procedure was shown by analyzing a cooling curve having several small deviations from the expected curve shape for a polymer, and providing a reasonable wide temperature range of the melt to extrapolate from.

Finally, in order to verify the consistency of the proposed corrections, both methods were applied (in cooling by the "Extrapolation method" and heating by the "Reference method") to three different dispersions of MA-g-PP in water, from where the enthalpies of transition and the evolution of the crystallinity were calculated. These results suggest that the two correction methods lead to fairly good estimations of the sought data.

Acknowledgements J.I. is indebted to the European Community for a Marie Curie Industry Host Fellowship grant, Contract Nr HPMI-CT-1999-00058. He would also like to thank DSM Research, the Katholieke Universiteit Leuven, and SciTe B.V. for scientific and financial support. Also, support for V.M. from the FP7 CSA project "NaPolyNet", see http://www.napolynet.eu, is valued.

References

1. Frensch H, Harnschfeger P, Jungnickel BJ. Fractionated crystallization in incompatible polymer blends. In: Utracki LA, Weiss RA, editors. Multiphase polymers: blends and ionomers. Washington: ACS Symposium Series; 1989. p. 101–125.
2. Vonnegut B. Variation with temperature of the nucleation rate of supercooled liquid tin and water drops. J Colloid Sci. 1948; 3(6):563–9.
3. Turnbull D. Formation of crystal nuclei in liquid metals. J Appl Phys. 1950;21:1022–8.

4. Cormia RL, Price FP, Turnbull D. Kinetics of crystal nucleation in polyethylene. J Chem Phys. 1962;37(6):1333–40.
5. Gornick F, Ross GS, Frolen LJ. Crystal nucleation in polyethylene: the droplet experiment. J Polym Sci C Polym Symp. 1967;18:79–91.
6. Koutsky JA, Walton AG, Baer E. Nucleation of polymer droplets. J Appl Phys. 1967;38(4):1832–9.
7. Groeninckx G, Vanneste M, Everaert V. Crystallization, morphological structure, and melting of polymer blends. In: Utracki LA, editor. Polymer blends handbook. New York: Kluwer Academic Publisher; 2003. p. 203–94.
8. Tol RT, Mathot VBF, Reynaers H, Groeninckx G. Relationship between phase morphology and crystallization behavior in crystallizable polymer blends: fractionated crystallization and homogeneous nucleation. In: Harrats C, Thomas S, Groeninckx G, editors. Micro- and nanostructured multiphase polymer blend systems: phase morphology and interfaces. Boca Raton: CRC Press, Taylor and Francis Group; 2006. p. 391–420.
9. Müller AJ, Balsamo V, Arnal ML. Nucleation and crystallization in diblock and triblock copolymers. Adv Polym Sci. 2005;190: 1–63.
10. Massa MV, Carvalho JL, Dalnoki-Veress K. Direct visualization of homogeneous and heterogeneous crystallization in an ensemble of confined domains of poly(ethylene oxide). Eur Phys J E. 2003;12:111–7.
11. Kailas L, Vasilev C, Audinot JN, Migeon HN, Hobbs JK. A real-time study of homogeneous nucleation, growth, and phase transformations in nanodroplets of low molecular weight isotactic polypropylene using AFM. Macromolecules. 2007;40:7223–30.
12. Turnbull D, Fisher JC. Rate of nucleation in condensed systems. J Chem Phys. 1949;17:71–3.
13. Barham PJ, Jarvis DA, Keller A. A new look at the crystallization of polyethylene. III. Crystallization from the melt at high supercoolings. J Polym Sci Part B Polym Phys. 1982;20(9): 1733–48.
14. Frensch H, Jungnickel BJ. Fractionated and self-seeded crystallization in incompatible polymer blends. Plast Rub Comp Proc Appl. 1991;16(1):5–10.
15. Everaert V, Groeninckx G, Aerts L. Fractionated crystallization in immiscible POM/(PS/PPE) blends part 1: effect of blend phase morphology and physical state of the amorphous matrix phase. Polymer. 2000;41(4):1409–28.
16. Arnal ML, Müller AJ, Maiti P, Hikosaka M. Nucleation and crystallization of isotactic poly(propylene) droplets in an immiscible polystyrene matrix. Macromol Chem Phys. 2000; 201(17):2493–504.
17. Tol RT, Mathot VBF, Groeninckx G. Confined crystallization phenomena in immiscible polymer blends with dispersed micro- and nanometer sized PA6 droplets, part 2: reactively compatibilized PS/PA6 and (PPE/PS)/PA6 blends. Polymer. 2005;46: 383–96.
18. He Y, Zhu B, Kai W, Inoue Y. Nanoscale-confined and fractional crystallization of poly(ethylene oxide) in the interlamellar region of poly(butylene succinate). Macromolecules. 2004;37(9): 3337–45.
19. Massa MV, Dalnoki-Veress K. Homogeneous crystallisation of poly(ethylene oxide) confined to droplets: the dependence of the crystal nucleation rate on length-scale and temperature. Phys Rev Lett. 2004;92(25):Art no. 255509.
20. Jin Y, Hilter A, Baer E, Masirek R, Piorkowska E, Galeski A. Formation and transformation of smectic polypropylene nanodroplets. J Polym Sci Part B Polym Phys. 2006;44(13):1795–803.
21. Ibarretxe J, Groeninckx G, Bremer L, Mathot VBF. Quantitative evaluation of fractionated and homogeneous nucleation of polydisperse distributions of water-dispersed maleic anhydride-grafted-polypropylene micro- and nano-sized droplets. Polymer. 2009;50(19):4584–95.
22. Müller AJ, Balsamo V, Arnal ML, Jakob T, Schmalz H, Abetz V. Homogeneous nucleation and fractionated crystallization in block copolymers. Macromolecules. 2002;35:3048–58.
23. Reiter G, Castelein G, Sommer JU. Direct visualization of random crystalization and melting in arrays of nanometer-size polymer crystals. Phys Rev Lett. 2001;87(22):Art no 226101.
24. Ibarretxe Uriguen J, Bremer L, Mathot VBF, Groeninckx G. Preparation of water-borne dispersions of polyolefins: new systems for the study of homogeneous nucleation of polymers. Polymer. 2004;45:5961–8
25. Wevers MGM. Full dissolution and crystallization of polyamides in water and other solvents. Doctoral Thesis by the Katholieke Universiteit Leuven. Leuven, Belgium. 2006.
26. Turnbull D, Cormia RL. Kinetics of crystal nucleation in some alkane liquids. J Chem Phys. 1961;34(3):820–31.
27. Montenegro R, Landfester K. Metastable and stable morphologies during crystallization of alkanes in miniemulsion droplets. Langmuir. 2003;19:5996–6003.
28. Tanden A, Landfester K. Crystallization of poly(ethylene oxide) confined in miniemulsion droplets. Macromolecules. 2003;36: 4037–41.
29. Weber CH, Chiche A, Krausch G, Rosenfeldt S, Ballauff M, Harnau L, Göttker-Schnetmann I, Tong Q, Mecking S. Single lamella nanoparticles of polyethylene. Nano Lett. 2007;7(7): 2024–9.
30. Wevers MGM, Mathot VBF, Pijpers TFJ, Goderis B, Groeninckx G. Full dissolution and crystallization of polyamide 6 and polyamide 4.6 in water and ethanol. In: Reiter G, Strobl GR, editors. Progress in understanding of polymer crystallization. Berlin: Springer; 2007. p. 151–68.
31. Wevers MGM, Pijpers TFJ, Mathot VBF. The way to measure quantitatively full dissolution and crystallization of polyamides in water up to 200 degrees C and above by DSC. Thermochim Acta. 2007;1(453):67–71.
32. Smith JM, Van Nes HC, Abott M. Introduction to chemical engineering thermodynamics. New York: McGraw-Hill;1996.
33. Mathot VBF. Thermal characterization of states of matter. In: Mathot VBF, editor. Calorimetry and thermal analysis of polymers. Munich, Vienna, New York: Hanser Publishers; 1994. p. 105–67.
34. Mileva D, Androsch R, Zhuraviev E, Schick C. Temperature of melting of the mesophase of isotactic polypropylene. Macromolecules. 2009;42(19):7275–8.
35. Pyda M, editor. The ATHAS Data Bank. http://athas.prz.rzeszow.pl.